LANGMUIR

Article

Dynamics of Microscale Liquid Propagation in Micropillar Arrays

Mohamed H Alhosani, and TieJun Zhang

Langmuir, **Just Accepted Manuscript** • Publication Date (Web): 31 May 2017

Langmuir is published by the American Chemical Society. 1155 Sixteenth Street N.W., Washington, DC 20036

Dynamics of Microscale Liquid Propagation in Micropillar Arrays

*Mohamed H. Alhosani, TieJun Zhang**

Department of Mechanical and Materials Engineering, Masdar Institute, Khalifa University of Science and Technology, P.O. Box 54224, Abu Dhabi, UAE

*Email: tjzhang@masdar.ac.ae

ABSTRACT

Understanding the dynamics of microscale liquid propagation in micropillar arrays can lead to significant enhancement in macroscopic propagation modeling. Such phenomenon is fairly complicated and fundamental understanding is lacking. The aim here is to estimate three main parameters in liquid propagation, capillary pressure, average liquid height and contact angle on pillar side, through modeling and experimental validation. We show that the capillary pressure is not constant during liquid propagation, and average capillary pressure is evaluated by using its maximum and minimum values. Average liquid height influences the permeability of such structure, which is challenging to determine due to complicated 3-D meniscus shape. A simple physical model is provided in this paper to predict average liquid height with less than 7% error. Contact angle on micropillar side, which have considerable impact on the capillary pressure and the average liquid height, have been debated for long time. We propose a model to predict this contact angle and validate it against experimental values in open literature. Our findings also

indicate that the microscopic motion of liquid front is significantly affected by the ratio of pillar height to edge-to-edge spacing, and a correlation is provided for quantification. The proposed models are able to predict the droplet spreading dynamics and estimate spreading distance and time reasonably.

KEYWORDS: Capillary pressure, Permeability, Contact angle, Wicking, Liquid propagation, Dynamic, Droplet spreading

1. INTRODUCTION

Liquid propagation (wicking) in porous media have been extensively studied owing to its application in variety of engineering applications such as thermal management of high heat flux devices, microfluidics and power generation. The advantage of such surfaces is that capillary pressure provides effective liquid transport mechanism for small devices. These surfaces can be produced by introducing micro/nanostructures on intrinsically hydrophilic surfaces based on Wenzel equation[1]. Among these surfaces, silicon micropillar arrays have been extensively studied to understand the fundamentals of liquid propagation[2–7]. Using photolithography technique and deep reactive ion itching (DRIE), precise pillar diameter, spacing and height can be manufactured which is crucial for fundamental understanding. Also, scalable and low-cost micro/nanostructured surface can be fabricated on metallic surfaces using different methods such as anodization[8,9], oxidation[3], electrochemical deposition[3,8] and biotemplated nanofabrication[10].

One of the early studies in liquid propagation was done by Washburn[11] to estimate liquid rise rate in capillary tubes. The model was obtained by balancing capillary pressure with viscous resistance, which was then extended to predict liquid propagation in porous media. The main challenge in such a problem is to estimate capillary pressure and viscous resistance (permeability). Recently, Xiao at al.[12] proposed semianalytical model to predict liquid propagation rate in micropillar array. The capillary pressure was determined by predicting the meniscus shape using energy minimization software called "*surface evolver*" and validated using interferometry (confocal microscope images). Brinkman's equation was solved numerically to obtain permeability. The model provides good predictions when the height to spacing ratio is larger than 1 and diameter to spacing ratio is lower than 0.57 and over-predicts outside this range. To overcome this problem, the same group[13] studied the microscale liquid propagation dynamics

in which the liquid propagation between two pillars (sweeping) was analyzed. The results show the importance of accounting microscale dynamics, especially in sparse structures. They also show that the sweeping distance scales with one-fifth power of time. Another study done by Tanner suggests that the sweeping distance scales with one-seventh power of time[14].

M. Rahman et al.[10] studied the effect of liquid propagation rate on critical/dry-out heat flux. Propagation rate was measured with high speed imaging of liquid drawn from a 500μm capillary tube when in contact with the surface. The results show that liquid propagation rate is the single main factor that determines the dry-out heat flux on structured superhydrophilic surfaces. Optimization of liquid propagation on square micropillar arrays was done by Hale et al.[15] based on several models and numerical simulations. It was found that for a given aspect ratio, there exists an optimum pillar spacing that provides the maximum flow rate. Another group also presented the dynamics of liquid propagation in nanopillars[16] and reported that pillar structures have significant influence on the propagation process. The modeling results were then validated with experimental data from literature. Antao et al.[17] provided simple yet accurate capillary pressure model based on the force balance in a unit cell of micropillar array. The model was used to estimate the maximum propagation rate, which is also a representation of dryout heat flux on such surfaces[18].

Despite the huge effort directed to understand the liquid propagation in micro/nanostructured surfaces, this phenomenon is still unclear and different models produce various results as shown by Horner et al.[4] and Ravi et al.[19,20]. For instance, microscopic sweeping process is still vague and physical insight of this process can lead to significant improvement in macroscopic behavior. Also, an important parameter to understand liquid propagation is the contact angle on the pillar side, which was determined by interferometry by Antao et al.[17] for water on silicon to be much

larger than equilibrium contact angle. Also, Ravi et al.[19,20] used a contact angle of 56° when simulating water propagation on silicon micropillar array. On the other hand, Zhu et al.[18] used a contact angle of 30°. This shows that a model that can predict contact angle of liquid on micropillar side is lacking in literature.

Another important parameter that affect liquid propagation rate is the permeability. One of the early studies to estimate permeability of micropillar array is done by Sangani and Acrivos in 1982[2]. The proposed numerical model assumes flat meniscus (contact angle = 90°) between the pillars which lead to over-prediction of permeability since the flow area is larger. The effect of meniscus curvature was taken into account on Byon and Kim[3] permeability model in which the surface energy minimization tool was used to obtain general correlation for average meniscus height. One main drawback is that this correlation can be significantly off if the parameters used is not within the range of the correlation. Recently, Zhu, et al.[18] proposed that the meniscus height/curvature is changing from the liquid supply point along the wicking direction. Basically, the pressure difference in wicking system is due to curvature difference. This change in curvature results in different meniscus heights along the flow. Therefore, a simple universal model is needed to accurately predict average (effective) meniscus height within a unit cell as a function of pillar diameter, spacing, height and contact angle.

In this paper, we show that capillary pressure during propagation and sweeping is not constant and therefore, average capillary pressure is proposed based on maximum and minimum capillary pressure. Also, a model that can predict contact angle on micropillar sidewall was produced, and validated against interferometry measurements from literature. Furthermore, we provide a simple yet accurate model to estimate average liquid height in a unit cell which is crucial for permeability estimation. Finally, average capillary pressure, average liquid height and contact

angle models were validated using liquid rise and droplet spreading experiments on silicon micropillar arrays.

2. RESULTS AND DISCUSSION

In this work, we study the liquid propagation in hydrophilic micropillar arrays. A scanning electron microscope (SEM) image of such sample with pillar diameter of d, center-to-center spacing (pitch) of p and pillar height of h is shown in Figure 1a. The aim is to estimate the spreading time and spreading diameter when a liquid droplet is deposited in such surfaces (Figure 1b), also to predict the liquid propagation rate when such surface comes in contact with liquid reservoir as shown in Figure 1c.

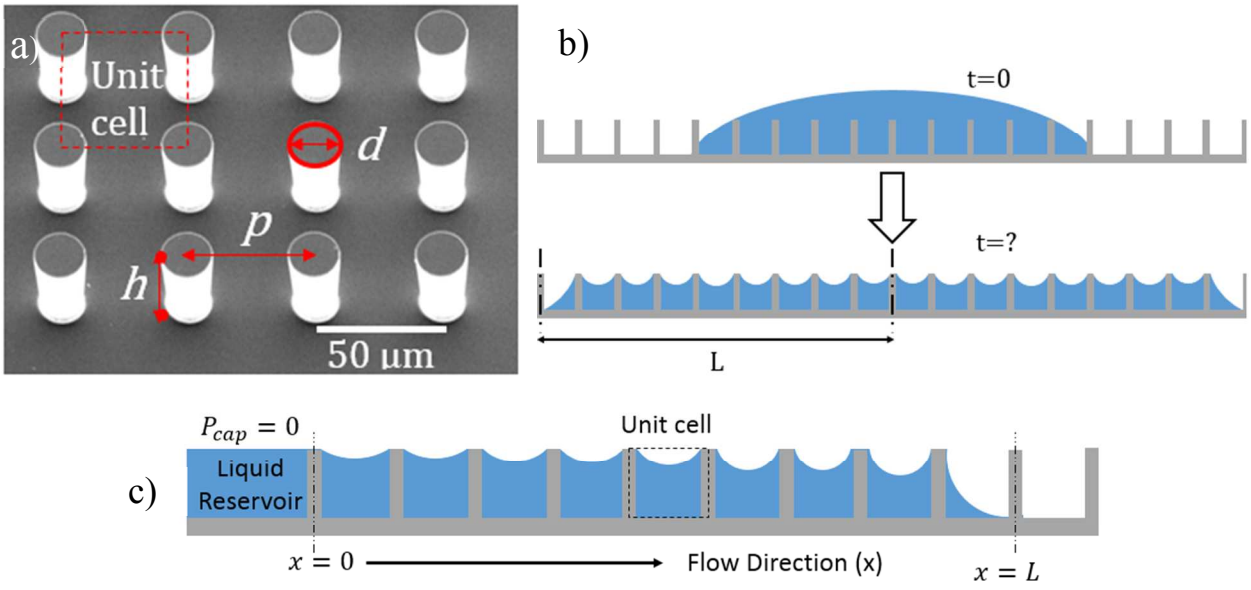

Figure 1. a) SEM image of fabricated sample with diameter d, pitch p and height h, b) schematics of droplet spreading in micropillar arrays, c) side view schematics of liquid propagation in micropillar arrays.

Darcy's law for flow in porous media can be used to simulate this problem,

$$\dot{m}_{prop} = -\frac{\rho K A}{\mu}\frac{dP}{dx} \quad (1)$$

where, $\dot{m}_{prop}$ is liquid mass flow rate, ρ is liquid density, K is permeability, A is liquid flow area and μ is liquid viscosity. The driving pressure in this case is the capillary pressure (P_{cap}),

$$\frac{dP}{dx} = \frac{(P_{atm} - P_{cap})_{@\,x=L} - (P_{atm} - P_{cap})_{@\,x=0}}{L} \quad (2)$$

where L is the propagating distance from liquid reservoir. To estimate liquid propagation rate, we need to get the permeability and capillary pressure.

3.1 Average capillary pressure in micropillar arrays

When liquid is moving from one row of pillars to the next one, the capillary pressure is not constant. For instance, the maximum capillary pressure is just after the liquid wets the micropillars, and the minimum capillary pressure (P_{min}) is just before the liquid wets the next row of pillars. Applying the force balance in a unit cell of micropillar arrays suggests that capillary pressure follows the equation below (see Supporting Info. S-1 for derivation)

$$P_{cap}(x) = \frac{\sigma\frac{\pi d}{2}cos\theta_{adv} - p\sigma sin\theta_{adv}}{p(\frac{d}{2} + x) - \frac{\pi d^2}{8}} \quad (3)$$

where θ_{adv} is the advancing contact angle and x is the distance from the pillar edge to the liquid front. Note that pressure difference (ΔP) in Figure 2 is equals to P_{cap}. Due to DRIE process, scallop like structures are formed on the pillar side, which should results in a lower contact angle based on Wenzel equation. However, high-resolution SEM images show that pillar side roughness is equal to 1.01 – 1.02, which can be neglected (see Supporting Info. S-1 for image). Other studies also show similar results such as Ayon et al.[21]. However, this roughness can be changed by changing DRIE process parameters.

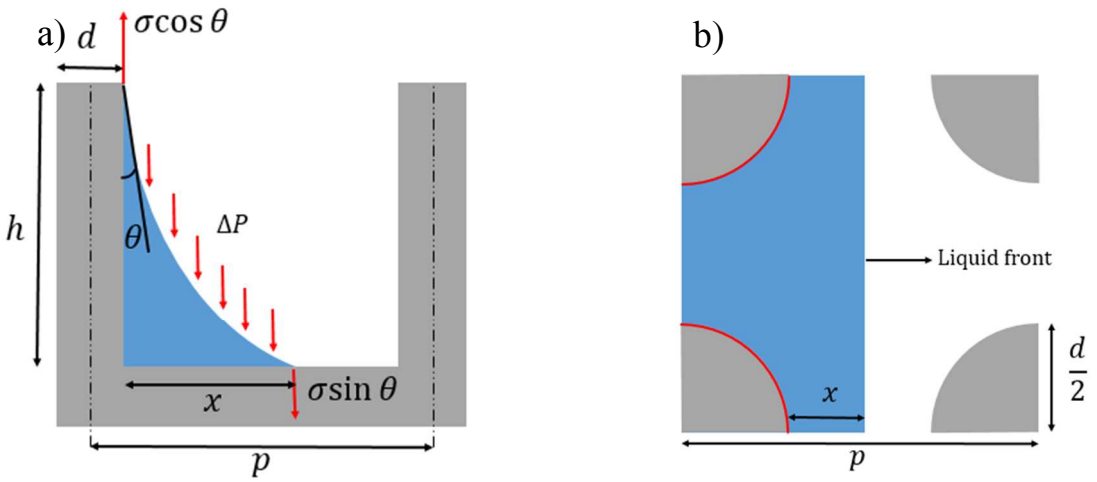

Figure 2. a) Side view, b) top view of liquid front and forces on the meniscus during sweeping process.

We define P_{max} when the liquid front at $x = 0$ and P_{min} when $x = p - d$ as shown in Figure 3.

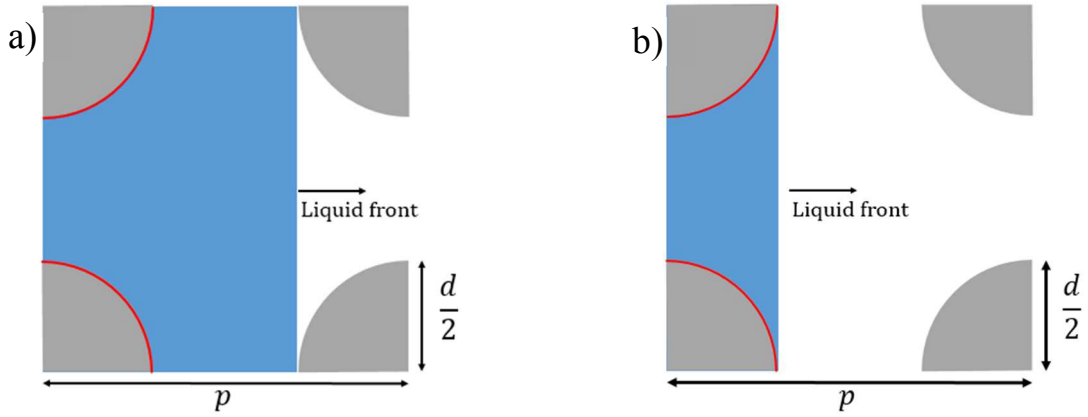

Figure 3. Top view of liquid front location when capillary pressure equal to a) P_{min}, b) P_{max}.

Substituting the value of x in Eq. (3), P_{min} and P_{max} can be calculated as shown in Eq. (4) and Eq. (5), respectively.

$$P_{min} = \frac{\sigma \frac{\pi d}{2} cos\theta_{adv} - p\sigma sin\theta_{adv}}{p\left(p - \frac{d}{2}\right) - \frac{\pi d^2}{8}} \quad (4)$$

$$P_{max} = \frac{\sigma \frac{\pi d}{2} cos\theta_{adv} - p\sigma sin\theta_{adv}}{p(\frac{d}{2}) - \frac{\pi d^2}{8}} \quad (5)$$

The above model does not takes into account the effect of pillar height on capillary pressure because it did not appear in the force balance directly. Previous studies reported over-estimation of capillary pressure when short pillars are modeled[13]. The main parameter here is the ratio of pillar height to edge-to-edge spacing (h/(p-d)). When h/(p-d) < 1, the capillary pressure is over-estimated. The reason is that the contact angle on pillar side (θ_{pillar}) is not the same as θ_{adv} for short pillars. Basically, for very short pillars, it is physically impossible to have θ_{adv} on both the bottom surface and pillar side as shown in Figure 4.

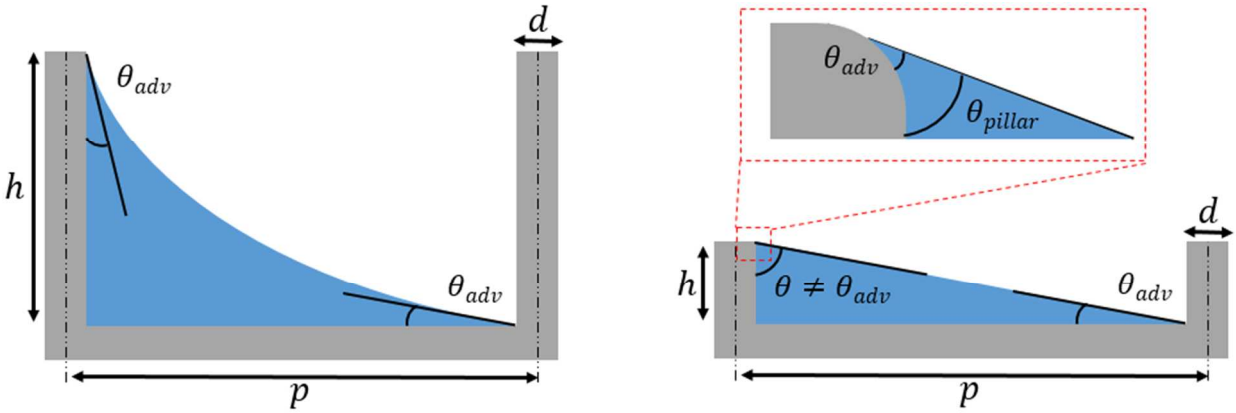

Figure 4. Liquid meniscus and contact angle on long and short pillars.

To estimate θ_{pillar} from h/(p-d), two boundary conditions are used. If h = (p-d), both bottom surface and pillar side contact angle will equal to θ_{adv}. On the other hand, if pillar height approaches zero, θ_{pillar} will approach (90+θ_{adv}). Note that contact angle on pillar wall can be larger than θ_{adv} due to the edge effect on pillar top, which does not exist on the bottom surface as shown in Figure 4. Based on these two boundaries, an approximation is developed to estimate θ_{pillar} from h/(p-d) as shown below

$$\theta_{pillar} = 90 - 2\tan^{-1}(\frac{h}{p-d}) + \theta_{adv} \quad (6)$$

Since θ_{pillar} cannot be lower than θ_{adv}, max[$\theta_{pillar,}$ θ_{adv}] is substituted in the first term of Eq. (3) and Eq.(5). During the liquid propagation process, the average capillary pressure can be determined from the time average of the pressure along *x*. Previous study by Xiao et al.[13] shows that the liquid front location (*x*) is a function of $t^{1/5}$, where *t* is time. However, Tanner reported that *x* is function of $t^{1/7}$. The first study which states sweeping distance scaling as $t^{1/5}$ was done on silicon micropillar arrays. The second study on the other hand, was on smooth surface. In the case of silicon micropillar arrays, the meniscus is pinned at the pillar top with constant height, while in the second case the liquid thickness decreases. This implies that pillar height affect the sweeping distance scaling (β). Therefore, six samples are tested and the liquid (water) sweeping on plasma cleaned silicon micropillar arrays samples with $h/(p-d)$ ranges between 0.5 to 1.6 are recorded with high speed camera at 5000 frames per second. It was found that $h/(p-d)$ strongly affect β and a correlation is developed to estimate β from $h/(p-d)$ as shown below. While this correlation is valid for the experimented range of $h/(p-d)$, we do not expect β to keep increasing. There is a physical limitation in which β cannot go beyond that will be discussed later in this manuscript.

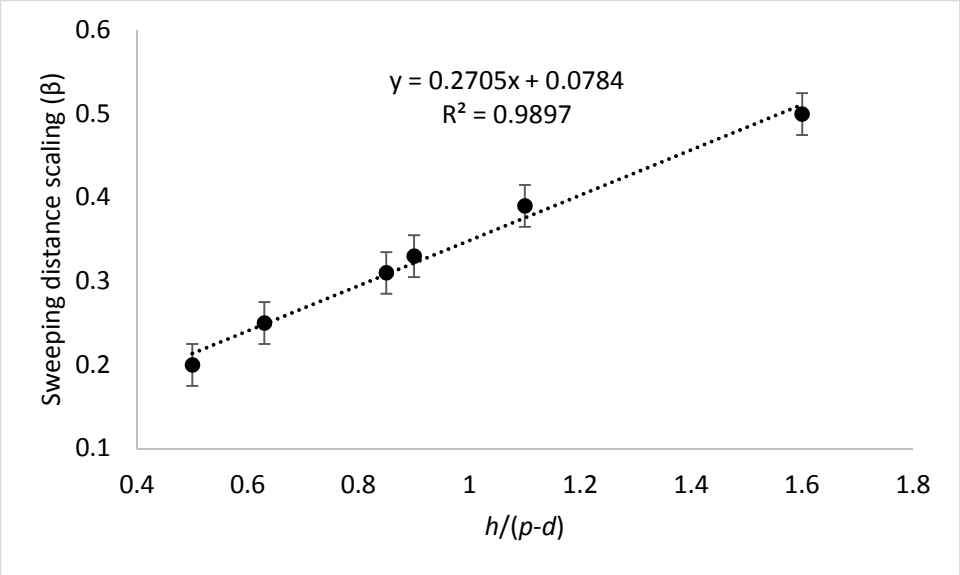

Figure 5. Sweeping distance scaling (β) vs. $h/(p\text{-}d)$.

$$\beta = 0.2705\left(\frac{h}{p-d}\right) + 0.0784 \tag{7}$$

Using this information, the average capillary pressure (P_{avg}) can be determined as shown below (see Supporting Info. S-3 for derivation)

$$P_{avg} = \sum_{i=1}^{i=\frac{t_s}{dt}} \frac{A}{Bt(i)^{\beta} + C} dt \tag{8}$$

$$A = \sigma\frac{\pi d}{2}cos\theta_{pillar} - p\sigma sin\theta_{adv}, \quad B = p(p-d), \quad C = \frac{pd}{2} - \frac{\pi d^2}{8}$$

The above model was for the edge unit cells. If we consider a unit cell with all 4 pillars wetted (center unit cell), the capillary pressure can be determined as that in[17] (see Supporting Info. S-2 for more details)

$$P_{center} = \frac{4\sigma cos\theta}{d\left(\frac{4}{\pi}\left(\frac{p}{d}\right)^2 - 1\right)} \tag{9}$$

We can use the above results to explain different phenomena such as liquid receding mechanism in micropillar arrays. Considering silicon micropillar array with d = 25, p = 65 and h = 36μm, and the contact angle of plasma cleaned silicon/silicon dioxide is about 2°, the capillary pressure vs. liquid front location (x) is illustrated in Figure 6.

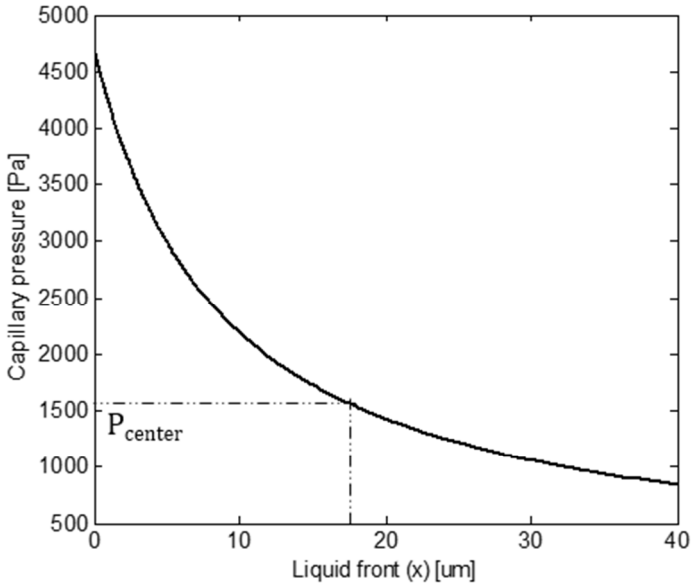

Figure 6. Capillary pressure variation in edge unit cell for d = 25, p = 65, h = 36 μm and θ_{eq} = 2°.

From Figure 6, during evaporation and liquid front receding process, liquid front (x) cannot be below the point that generate capillary pressure equals to $P_{center,\ max}$ (P_{center} with θ = receding contact angle (θ_{rec})) which in this case equal to 17 μm. The reason is that when looking at the unit cell just before the edge unit cell (let's call it "unit cell A" in Figure 7a) which has four pillars wetted with water, the maximum capillary pressure that can be generated is $P_{center,\ max}$. Assuming negligible pressure drop between the unit cell A and edge unit cell, the liquid front in the edge unit cell will recede till it reaches the point where the capillary pressure in the edge unit cell is equal to the maximum capillary pressure of unit cell A, which is $P_{center,\ max}$. At this point, liquid front in the edge unit cell will stop receding, and meniscus will de-pin and recede from

pillar top in the unit cell A till the bottom of the meniscus touches the substrate bottom surface as shown in Figure 7a and Figure 8. The analysis also indicates that drying process similar to Figure 7b is not possible. The reason is that in order to completely remove liquid from edge unit cell, the pressure in the unit cell A should be larger than P_{max} which is not possible.

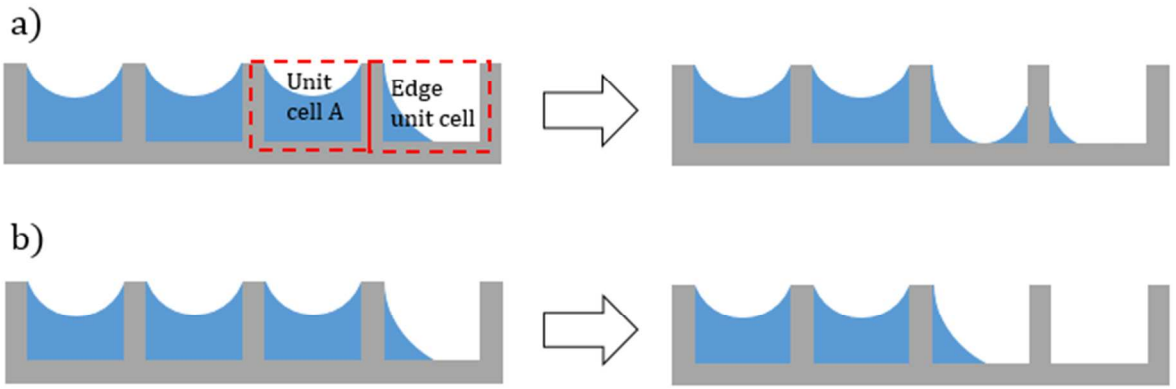

Figure 7. Dynamics of drying of micropillar array surface a)possbile, b) not possbile.

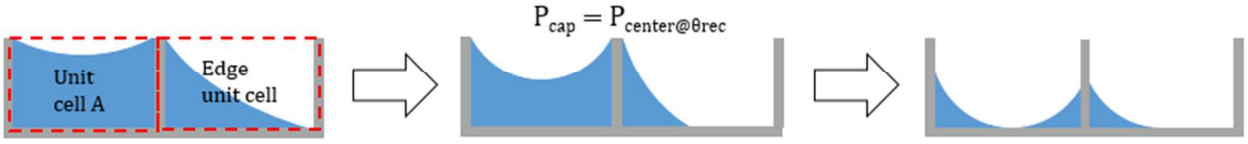

Figure 8. Dynamics of liquid drying/receding.

Experimental observations also support this as shown in Figure 9. The optical microscope images were taken after depositing water droplet on the surface and waiting for about a minute till the drying process is observed. Liquid front distance, x, was measured to be about 16μm in this experiment, which validate capillary pressure model. Also, the proposed drying process in Figure 7a agrees with the experimental drying process in Figure 9.

The same argument can be used to estimate the maximum sweeping distance scaling (β_{max}) which is to make $P_{avg} = P_{center,\ max}$ and solve for β. Therefore, for the tested sample above, $\beta_{max} \sim$ 0.75.

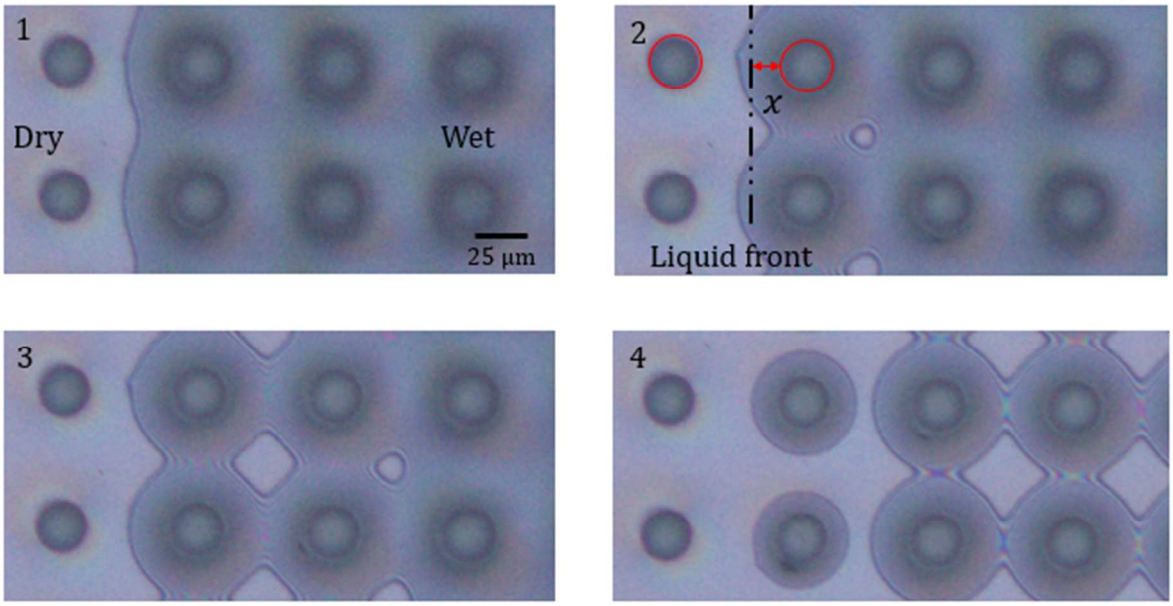

Figure 9. Optical microscope images of dynamic liquid front receding in micropillar array surface, $d = 25$, $p = 65$, $h = 36$ µm and $\theta_{adv} = 2°$.

One particular importance of $P_{center,\,max}$ is that it determines the capillary pressure at dry-out heat flux for cooling applications[18]. Basically, the liquid is pumped by capillary pressure from the liquid pool to the heated section, and cooling is happening by evaporation of liquid in the heated section. The maximum cooling capacity of such device is a direct function of the maximum liquid supply rate, that is when $P_{cap} = P_{center,\,max}$. The analysis in this paper suggests that the capillary pressure in propagating liquid (P_{avg}) is different than the capillary pressure of a receding liquid ($P_{center,\,max}$). Since P_{center} is relatively easier to estimate because the liquid front motion (x vs. t) is not required, a correlation was developed to estimate P_{avg} from $P_{center,\,max}$, $h/(p-d)$ and porosity (ε) (see Supporting Info. S-3 for details)

$$P_{avg} = P_{center,max}\left[0.469 + \frac{0.774h}{p-d} - 0.3582\varepsilon - 0.3\left(\frac{h}{p-d}\right)^2 + 0.128\,\frac{\varepsilon h}{p-d} + 0.0176\varepsilon^2\right] \qquad (10)$$

$$\varepsilon = \frac{p^2 - \frac{\pi d^2}{4}}{p^2} \tag{11}$$

The correlation in Eq. (10) is valid for $0.35 < \varepsilon < 0.9$ and $0.5 < \frac{h}{p-d} < 1.6$ for structures similar to micropillar arrays and produces results with less than 5% error when compared to the solution in Eq. (10). Note that the disjoining pressure is neglected in this work due to relatively large length scale of the structures. To apply this model to nano-pillars and nano-wires with sub-micron length scale, order of magnitude analysis should be done to determine how significant disjoining pressure as compared to capillary pressure. Comparison between the capillary pressure model prediction of this work, Xiao et al.[12] and Srivastava et al. [22] is presented in Supporting Info. S-3.

3.2 Contact angle on pillar side

Now we will consider deposit a droplet on micropillar arrays. Liquid is propagated from the central region (droplet region) where pressure is equal to atmospheric pressure P_{atm} (capillary pressure ~ 0) to thinfilm region where pressure is equal to P_{atm} - P_{avg}. Steady state (no flow) happens when the pressure difference is zero. Therefore, the pressure on the edge unit cells calculated by Eq. (4) should equal to pressure in the middle region which is calculated using Eq. (9) with contact angle equal to steady-state contact angle (θ_{st}) as shown in Figure 10 below.

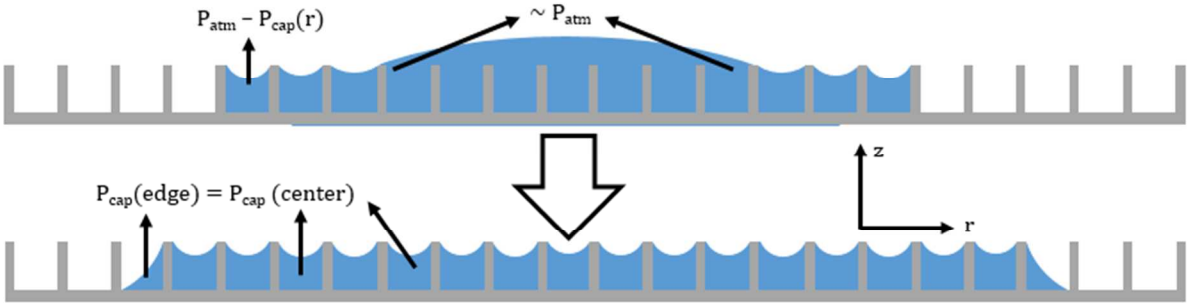

Figure 10. Droplet spreading on superhydrophilic micropillar array. Steady state happen when central pressure equal to edge pressure.

We have seen before that the edge capillary pressure is not constant and is fluctuating between P_{min} and P_{max}. Also, the capillary pressure in the central region is increasing from about 0 (when droplet is deposited and when we have flat meniscus) to the point that center pressure is equal to edge pressure. Steady state (no flow) happens when pressure different between edge and center is zero. The first point that will satisfy the no flow condition is when $P_{edge} = P_{min}$, which indicate that liquid front in the edge unit cell is as in Figure 3a, which is the minimum capillary pressure of the edge unit cell. Optical microscope visualization of liquid front directly after droplet deposition shows that the liquid front is very close to the next row of pillars (which produce P_{min}) as shown in Figure 11 that reflects the modeled scenario.

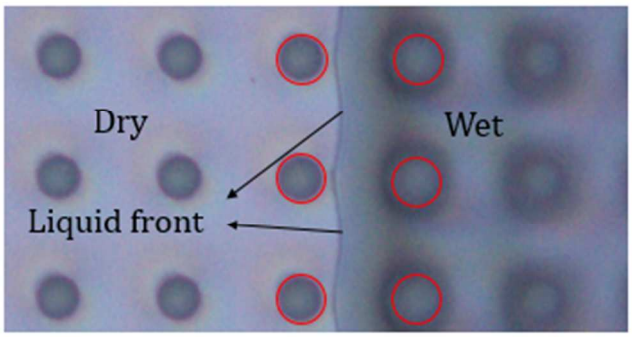

Figure 11. Optical microscope visualization of liquid front at steady state.

By making P_{min} ($\theta = \theta_{adv}$) in Eq. (4) = P_{center} ($\theta = \theta_{st}$) in Eq. (9), the θ_{st} in the middle region can be calculated as follows (see Supporting Info. S-2 for derivation)

$$\theta_{st} = \cos^{-1}\left(\frac{P_{min} d\left(\frac{4}{\pi}\left(\frac{p}{d}\right)^2 - 1\right)}{4\sigma}\right) \quad (12)$$

This is the contact angle at all pillars (except edge pillars in which $\theta = \theta_{adv}$) when the liquid stops propagating with negligible evaporation rate. This explains why the water contact angles on silicon micropillar sides is larger than the equilibrium contact angle on smooth silicon surface[4,17,19,20]. For example, Antao et al.[17] used confocal measurement to estimate contact angle on silicon micropillar, a value of 50 ± 4° was reported. Using the same pillar geometry, our model predicts a contact angle of 58°.

3.3 Average liquid height

To estimate the spreading diameter of a drop when deposited in micropillar arrays, and to estimate the permeability of such structure, the liquid height should be estimated. This can be achieved by applying horizontal force balance in a unit cell as shown in Figure 12 below.

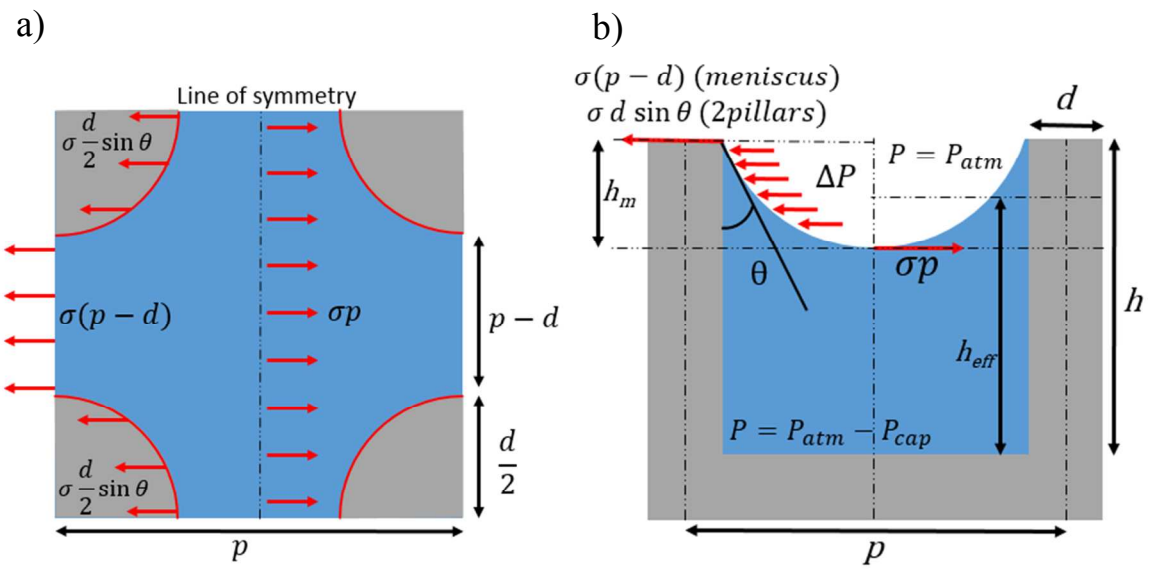

Figure 12. a) top view, b) side view of horizontal forces acting on half unit cell.

At steady state, forces toward the left should equal to forces toward the right, solving that will lead to (see supporting info. S-4 for derivation)

$$h_m = \frac{\sigma(1-sin\theta)}{P_{cap}}\left(\frac{d}{p}\right) \tag{13}$$

where h_m is menicus height. The effective meniscus height from bottom surface is

$$h_{eff} = \left(h - \frac{h_m}{2}\right) \tag{14}$$

To validate our model in Eq. (13) and Eq. (14), four silicon micropillar array samples were fabricated, and four experiments were done for each sample. So, each experimental result in Table 1 is the average of four experiments. Before experiment, the sample is cleaned with acetone, IPA , water and 20 minutes plasma cleaning. The contact angle after plasma cleaning was measured to be around 2°. Droplet is generated using 32G size needle that can produce droplet size ranging from 1 – 3 µL. To accurately measure droplet size, high speed camera was used to take side-view images of the droplet as shown in Figure 13a. The high speed camera video was also used to measure spreading time, which will be discussed in the next section.

Another camera was used to take top view image so that the final wetted are can be measured as in Figure 13b. The time between the droplet contacting the surface and top view image is about 2-3 seconds, and during this short period, evaporation is neglected. For instance, a 2 μL droplet needs more than 2 minutes to completely evaporate under lab condition. ImageJ software was used to measure the droplet volume (side view image) and wetted area (top view image). To estimate wetted area, liquid volume in each unit cell (V_{Lcell}) should be calculated using h_{eff} as shown below

$$V_{Lcell} = p^2 h_{eff} - \pi \left(\frac{d}{2}\right)^2 h_{eff} \tag{15}$$

Since this problem represents a steady state condition (no flow), contact angle on all pillars will equal to θ_{st}, which is substitute in Eq. (13). If the liquid volume in each unit cell is known, the final wetted area can be calculated from the initial droplet volume (V_i)

$$A_{wetted} = \frac{V_i}{V_{Lcell}} p^2 \tag{16}$$

Our model prediction is compared with Byon and Kim model[3] in Table 1, which shows significant improvement. Note that θ_{adv} is substituted in Byon and Kim model, and if θ_{st} is used instead, both model produce almost the same results with less than 7% error.

Table 1. Experimental and modeling results of liquid volume in a unit cell.

d, p, h (μm)	θ_{adv}	θ_{st}	Experimental V_{Lcell} (pL)	Modeled V_{Lcell} (pL)	% error	Byon & Kim V_{Lcell} (pL)[3]	% error
14, 36, 35.7	2	56.2	38.7 ± 1.0	39.0	0.9%	34.2	11.6%
19, 51, 35.6	2	56.5	73.4 ± 2.5	77.5	5.6%	63.6	13.4%
24, 66, 35.6	2	57.5	119.8 ± 2.1	128.3	7.1%	97.7	18.4%

34, 76, 37.9	2	55.4	160.2 ± 4.6	169.0	5.5%	126.2	21.2%

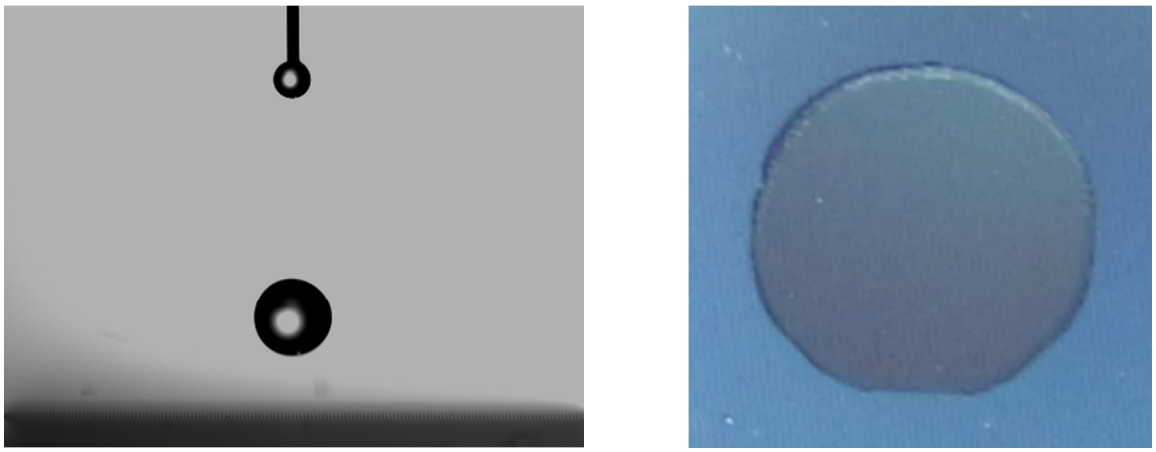

Figure 13. a) side view image with high speed camera, b) top view image of final wetted area.

3.4 Validation with capillary liquid rise experiment

P_{avg} and h_{eff} models can be validated using liquid rise rate experiments. However, h_{eff} is changing from the liquid pool to the liquid front as indicated by Zhu et al.[18]. For instance, at $z = 0$, we have a flat meniscus with zero capillary pressure and therefore, $h_{eff} = h$. At the other end where $z = L$, capillary pressure is equal to P_{avg} which is used to estimate contact angle using Eq. (12). After that, this contact angle is used to calculate h_{eff} using Eq. (13) and Eq. (14). An average value of h_{eff} is taken as shown below

$$h_{avg} = \frac{h + h_{eff}}{2} \tag{17}$$

h_{avg} was then substituted in Byon and Kim model to get the permeability[3]. Eq. (1) can be solved to get the propagation distance as a function of time as shown below

$$z = \sqrt{\frac{2KP_{avg}t}{\mu\varepsilon}} \tag{18}$$

where, z is propagation distance and t is time. The experiment starts when vertically oriented silicon micropillar arrays sample comes in contact with water pool. Note that gravity is neglected in this study since the capillary pressure for this structures is more than 10 times larger than the static head at maximum propagation distance. Propagation distance versus time was measured using high speed camera at 200 frames per second. Before experiment, the samples were cleaned with acetone, IPA, water then 20 minutes plasma cleaning. The experiments were done in lab condition with temperature ~ 25°C. Our models agrees with the experimental results with less than 10% error.

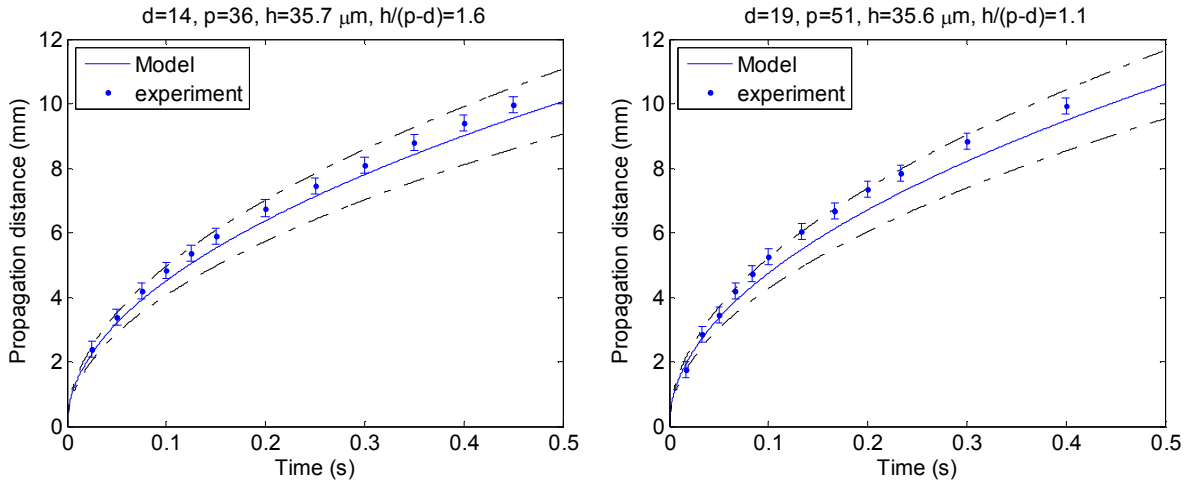

Figure 14. Propagation distance vs. time in micropillar arrays, a) d=14, p=36, h=35.7 μm, b) d=19, p=51, h=35.6 μm. Dashed lines are ±10% error.

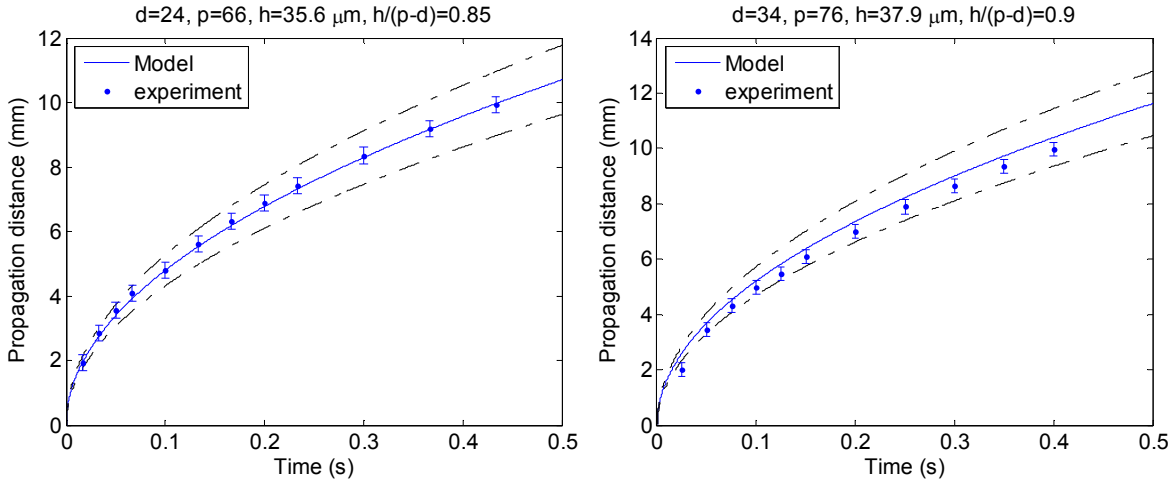

Figure 15. Propagation distance vs. time in micropillar arrays, a) d=24, p=66, h=35.6 μm, b) d=34, p=76, h=37.9 μm. Dashed lines are ±10% error.

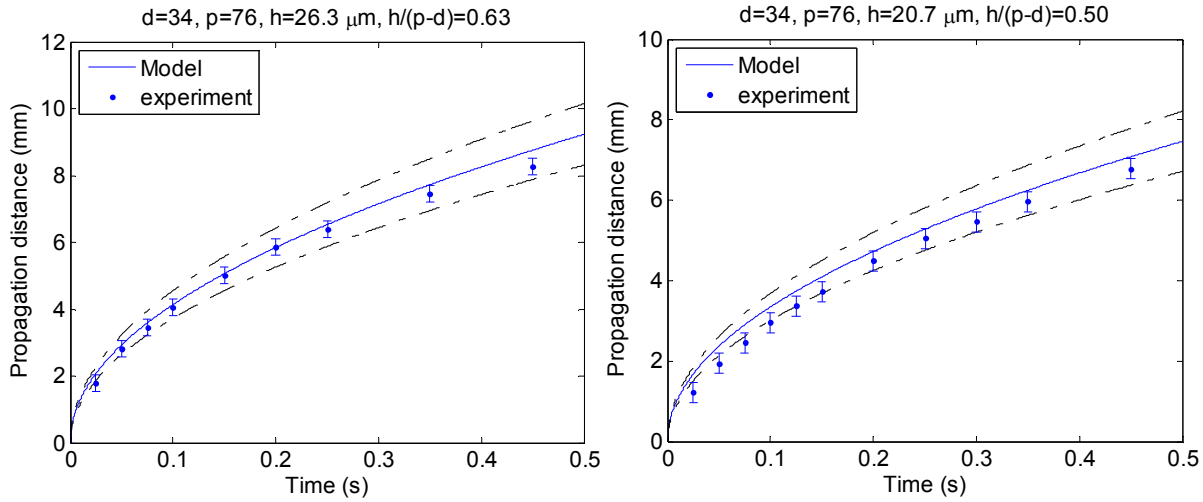

Figure 16. Propagation distance vs. time in micropillar arrays, a) d=35, p=75, h=26.3 μm, b) d=35, p=75, h=20.7 μm. Dashed lines are ±10% error.

3.5 Droplet spreading in silicon micropillar arrays

When a droplet is deposited on nano/microstructured surface, liquid propagates from droplet region to thinfilm region due to pressure difference. The liquid pressure in the droplet region is about the atmospheric pressure (P_{atm}), while in thinfilm region it is equal to P_{atm} - P_{cap}. This pressure difference drives the flow and steady state happens when the pressure on both sides are equal (no heating case). In this experiment, water droplet is deposited from close distance (2 cm) on dry, unheated microstructured surface to estimate the final wetted area and spreading time for a given droplet size and microstructure geometry.

To predict the spreading time of deposited droplet on microstructured surface, Eq. (1) is reformulated in cylindrical coordinate and divided by porosity to estimate interstitial velocity as shown below.

$$\frac{dL}{dt} = \frac{KP_{cap}}{\varepsilon\mu\, L\, ln\frac{L}{b}} \tag{19}$$

where L is the radius of circular wetted region and b is the radius of the droplet region as shown in Eq. (20) below

$$b = \left[\frac{3V_{drop}}{\pi}(2 - 3\cos(\alpha) + \cos^3(\alpha))\right]^{\frac{1}{3}} \sin(\alpha) \tag{20}$$

where α is the contact angle of the droplet region and is experimentally determined to be between 7° and 12° as shown in Figure 18b and Figure 18c, respectively. Figure 17 illustrates schematics of droplet spreading problem.

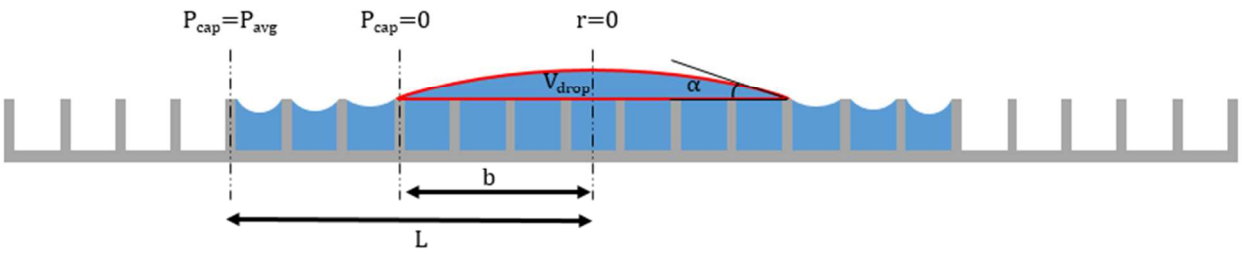

Figure 17. Schematic of droplet spreading on micropillar array surface.

Solution of Eq. (19) is shown in Supporting Info. S-5. The permeability in this case is similar to the one presented in the previous section of this report. At the edge of the droplet when $r=b$, the capillary pressure is equal to zero and therefore, $h_{eff} = h$. On the other hand, at the edge of wetted region at distance L, the capillary pressure is P_{avg}. The value of P_{avg} is used in Eq. (13) and Eq. (14). After that, Eq. (17) is used to calculate h_{avg} to estimate permeability with the Byon and Kim model[3].

The experimental procedure is similar to the one presented in "average liquid height" section. The high speed camera was set on 5000 frame per second. The needle height was kept at 2 cm to make Weber number constant. For instance, Weber number in our experiment was between 7.5 and 9 depending on the droplet size. These values of Weber number produces uncertainty in our experiments which are taken into account in droplet region contact angle (α). Figure 18 illustrates snapshots of high speed camera during liquid spreading to estimate the spreading time. It was observed that α is not constant and was changing from 7° (Figure 18b) to 12° (Figure 18c). This variation is due to initial droplet impingement (Weber number) which we tried to minimize in this experiment.

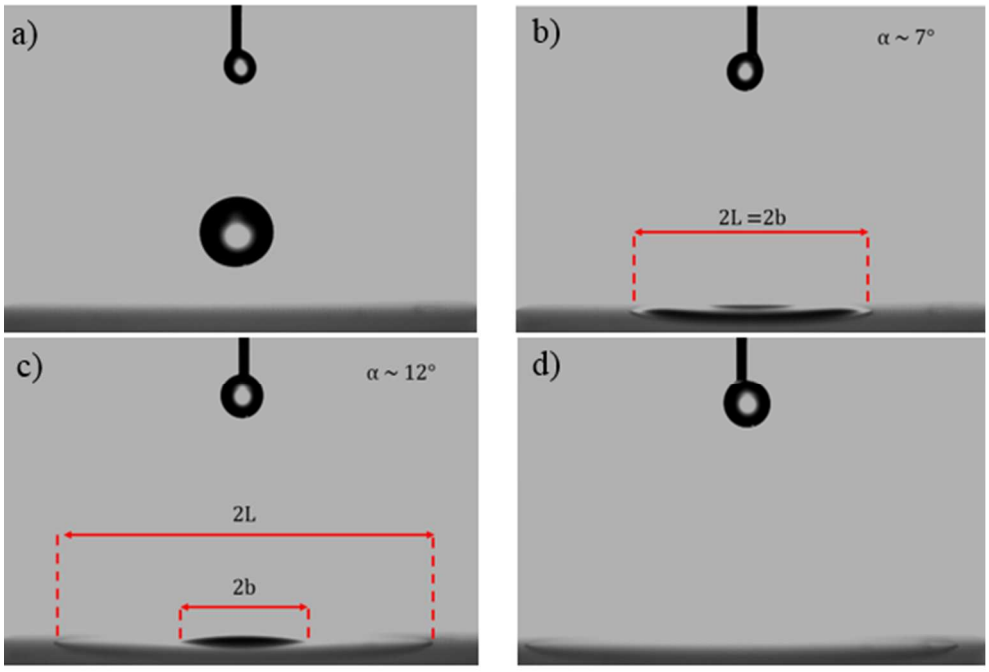

Figure 18. Snapshot of high speed camera for sample d=19, p=51, h=35.6μm. a) before impact, to measure initial droplet volume, b) t=0, c) t=30 ms, d) t=50.8 ms (full spreading).

Twelve similar experiments were done for four different samples to compare spreading time with the model prediction using P_{avg} and α = 7° and α = 12° as shown in Figure 19 and Table 2.

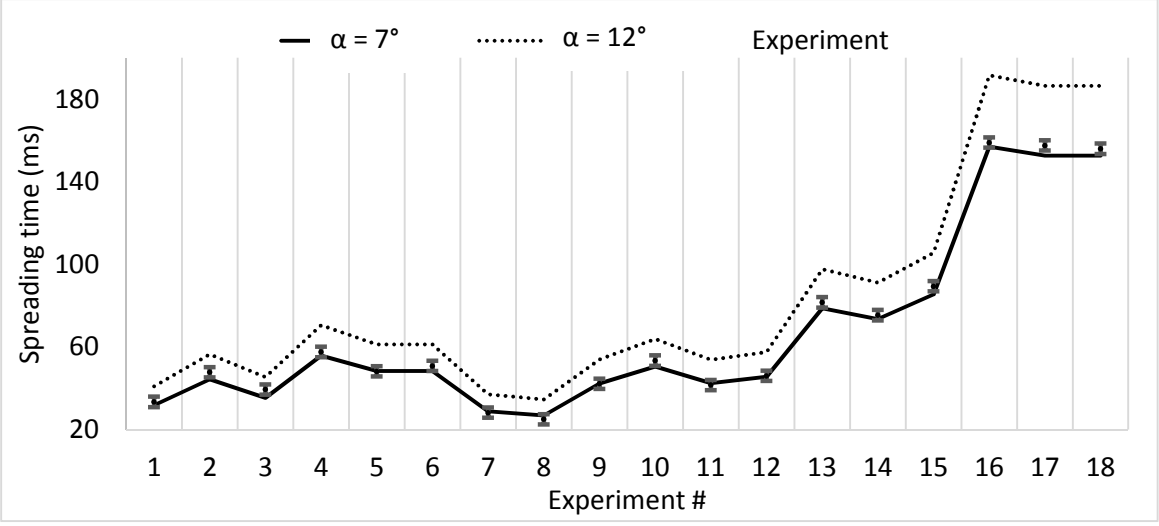

Figure 19. Comparison between experimental spreading time and model prediction.

Table 2. Experimental results of spreading time (ms) using different size droplet on different samples.

Exp. #	d (μm)	p (μm)	h (μm)	V_i (μL)	Modeled spreading time ($\alpha = 12°$)[ms]	Modeled spreading time ($\alpha = 7°$)[ms]	Spreading time (exp.) [ms]
1	14	36	35.7	1.33	40.9	31.8	33.4
2				1.74	56.5	44.4	47.8
3				1.45	45.4	35.4	39.4
4	19	51	35.6	2.28	70.5	55.8	57.6
5				2.03	61.3	48.3	48.2
6				2.03	61.3	48.3	50.8
7	24	66	35.6	1.36	37.1	28.9	28.2
8				1.28	34.5	26.8	25
9				1.85	53.9	42.3	42.2
10	34	76	37.9	2.43	63.8	50.6	53.4
11				2.11	53.8	42.5	41.6
12				2.23	57.5	45.5	46
13	34	76	26.3	1.44	97.6	78.7	81.6
14				1.36	91.2	73.4	75.4
15				1.54	105.6	85.4	89.4
16	34	76	20.7	1.30	191.5	157	159
17				1.27	186.4	152.7	157.6
18				1.27	186.4	152.7	156

Comparing the experimental results with the model prediction, the experimental results fits the model with $\alpha = 7°$, which means that the model slightly under-predict spreading speed. The main reason is that the propagation mechanism in this case is different from that of liquid rise experiment as shown in Figure 20.

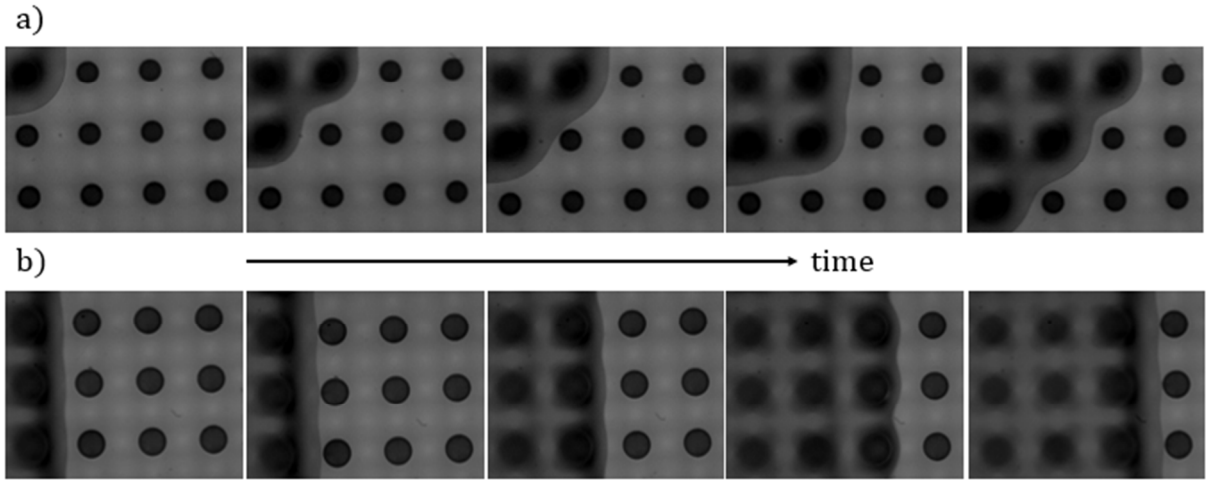

Figure 20. Propagation mechanism in a) droplet spreading, b) liquid rise.

The proposed capillary pressure model in this paper was based on the propagation mechanism similar to Figure 20b, where the liquid front motion parallels the pillars direction, as the case of liquid rise. In the case of droplet spreading, the liquid spread in all directions, which results in a microscale propagation mechanism similar to Figure 20a, and this leads to three wetted pillars instead of two wetted pillars per unit cell during microscale liquid propagation. As a result, P_{min} will be different as shown below

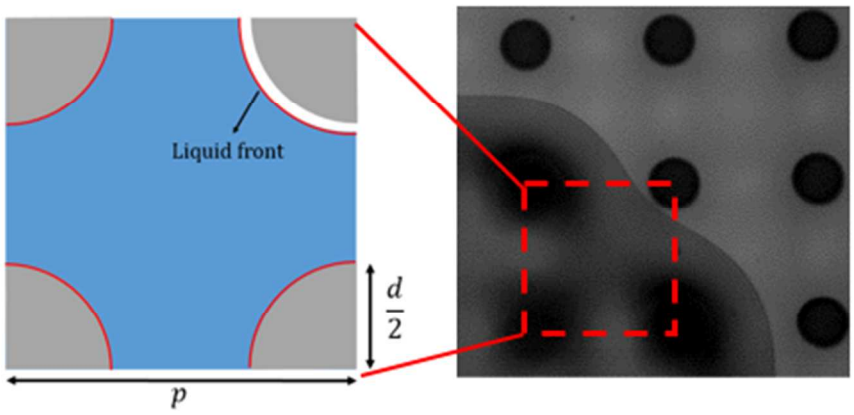

Figure 21. Schematics and microscope image of a unit cell that generates minimum capillar pressure with 3 wetted pillars.

$$P_{min3} = \frac{\sigma \frac{3}{4}\pi d cos\theta_{pillar} - d sin\theta_{adv}}{p^2 - \frac{\pi d^2}{16}} \quad (21)$$

Comparing the minimum capillary pressure when the liquid wets two pillars (P_{min}) and three pillars (P_{min3}), P_{min3} is 15% - 25% larger than P_{min} for the pillars geometry used in our experiments. The average capillary pressure in the case of three wetted pillars is difficult to estimate because the microscale liquid front motion (x vs. t) in unknown.

3. CONCLUSIONS

Liquid propagation in micropillar arrays has been studied in this paper in which three main parameters (capillary pressure, average liquid height and contact angle on pillar side wall) were estimated and validated with experimental data. It was shown that capillary pressure is not constant during liquid propagation and therefore, an average capillary pressure model was provided based on the maximum and minimum capillary pressure. Average liquid height in a unit cell, which is essential for permeability estimation, was modeled using the horizontal force balance analysis. A simple yet accurate model is developed. Contact angle on pillar sidewall was debated for long time in literature, we provided physical model to predict that. The contact angle model was validated with literature interferometry results. The modeling results agree with liquid rise experiments with less than 10% error. Previous studies suggested constant value of liquid sweeping scaling (β), our results show that it is significantly affected by $h/(p-d)$ Also, droplet spreading on silicon micropillar arrays was modeled, where the spreading time and diameter were estimated and validated. It was shown that due to different microscale propagation mechanism, the capillary pressure in droplet spreading case is higher than that in liquid rise, which stress on the importance of microscale propagation on macroscale propagation. This work

provides fundamental understanding of liquid propagation in micropillar arrays which is important to design capillary pumped devices.

4. ACKNOWLEDGEMENT

This work was supported by the cooperative agreement between Masdar Institute of Science and Technology, UAE, and the Massachusetts Institute of Technology (MIT), USA. Reference Number 02/MI/MIT/CP/11/07633/GEN/G/00. It was also supported by Abu Dhabi National Oil Company (ADNOC). The author appreciate the technical support from Mr. Leslie George at the Masdar Institute Clean Room.

5. SUPPORTING INFORMATION

Supporting information, including figures and equations for vertical force balance on edge unit cell, steady state contact angle on pillar side, average capillary pressure, average liquid height in a unit cell of micropillar arrays, and droplet spreading are available free of charge.

6. REFERENCES

(1) Wenzel, R. N. Resistance of Solid Surfaces to Wetting by Water. *J. Ind. Eng. Chem. (Washington, D. C.)* **1936**, *28*, 988–994.

(2) Sangani, A. S.; Acrivos, A. Slow Flow Past Periodic Arrays of Cylinders with Application to Heat Transfer. *Int. J. Multiph. Flow* **1982**, *8* (3), 193–206.

(3) Byon, C.; Kim, S. J. The Effect of Meniscus on the Permeability of Micro-Post Arrays. *J. Micromech. Microeng.* **2011**, *21*.

(4) Horner, D.; Ravi, S.; Moghaddam, S. Monoporous Micropillar Wick Structures, II-Optimization & Theoretical Limits. *Appl. Therm. Eng.* **2014**, *73* (1), 1378–1386.

(5) Raj, R.; Adera, S.; Enright, R.; Wang, E. N. High-Resolution Liquid Patterns via Three-Dimensional Droplet Shape Control. *Nat. Commun.* **2014**, *5*, 4975.

(6) Ranjan, R.; Patel, A.; Garimella, S. V.; Murthy, J. Y. Wicking and Thermal Characteristics of Micropillared Structures for Use in Passive Heat Spreaders. *Int. J. Heat Mass Transf.* **2012**, *55* (4), 586–596.

(7) Adera, S.; Antao, D.; Raj, R.; Wang, E. N. Design of Micropillar Wicks for Thin-Film Evaporation. *Int. J. Heat Mass Transf.* **2016**, *101*, 280–294.

(8) Lu, H.; Yan, K.; Yan, J.; Wang, J.; Huang, B. Fabrication of Copper Micro-Tubes by Electroless Deposition with an Etched Porous Aluminum Template without Using Sensitization and Activation. *Mater. Chem. Phys.* **2008**, *110* (1), 136–139.

(9) Piao, Y.; Lim, H.; Chang, J. Y.; Lee, W.-Y.; Kim, H. Nanostructured Materials Prepared by Use of Ordered Porous Alumina Membranes. *Electrochim. Acta* **2005**, *50*, 2997–3013.

(10) Auch, J. A. E. R. The Role of Wickability on the Critical Heat Flux of Structured Superhydrophobic Surfaces. *Rev. Lit. Arts Am.* **1999**, *178* (August), 173–178.

(11) Washburn, E. W. The Dynamics of Capillary Flow. *Phys. Rev.* **1921**, *17* (3), 273–283.

(12) Xiao, R.; Enright, R.; Wang, E. N. Prediction and Optimization of Liquid Propagation in Micropillar Arrays. *Langmuir* **2010**, *26* (19), 15070–15075.

(13) Xiao, R.; Wang, E. N. Microscale Liquid Dynamics and the Effect on Macroscale Propagation in Pillar Arrays. *Langmuir* **2011**, *27* (17), 10360–10364.

(14) Tanner, H. L. The Spreading of Silicon Oil Drops on Horizontal Surfaces. *J. Phys. D. Appl. Phys.* **1979**, *12* (9), 1473.

(15) Hale, R. S.; Bonnecaze, R. T.; Hidrovo, C. H. Optimization of Capillary Flow through Square Micropillar Arrays. *Int. J. Multiph. Flow* **2014**, *58*, 39–51.

(16) Mai, T. T.; Lai, C. Q.; Zheng, H.; Balasubramanian, K.; Leong, K. C.; Lee, P. S.; Lee, C.; Choi, W. K. Dynamics of Wicking in Silicon Nanopillars Fabricated with Interference Lithography and Metal-Assisted Chemical Etching. *Langmuir* **2012**, *28* (31), 11465–11471.

(17) Antao, D. S.; Adera, S.; Zhu, Y.; Farias, E.; Raj, R.; Wang, E. N. Dynamic Evolution of the Evaporating Liquid-Vapor Interface in Micropillar Arrays. *Langmuir* **2016**, *32* (2), 519–526.

(18) Zhu, Y.; Antao, D. S.; Lu, Z.; Somasundaram, S.; Zhang, T.; Wang, E. N. Prediction and Characterization of Dry-out Heat Flux in Micropillar Wick Structures. *Langmuir* **2016**, *32* (7), 1920–1927.

(19) Ravi, S.; Horner, D.; Moghaddam, S. A Novel Method for Characterization of Liquid Transport through Micro-Wicking Arrays. *Microfluid. Nanofluidics* **2014**, *17* (2), 349–357.

(20) S.Ravi,D. Horner, S. M. Monoporous Micropillar Wick Structures, I-Mass Transport Characteristics. *Appl. Therm. Eng.* **2014**, *73* (1), 1371–1377.

(21) Ayon, A. A.; Chen, K. S.; Lohner, K. A.; Sprearing, S. M.; Sawin, H. H.; Schmidt, M. A. Deep Reactive Ion Etching of Silicon. In *Materials Research Society Syimp.*; 1999; Vol. 546, pp 51–61.

(22) Srivastava, N.; Din, C.; Judson, A.; Macdonald, N. C.; Meinhart, C. D. A Unified Scaling Model for Flow through a Lattice of Microfabricated Posts †. *Lab Chip* **2010**, *10*, 1148–1152.

Table of Contents Graphic

Dynamics of Microscale Liquid Propagation in Micropillar Arrays

*Mohamed H. Alhosani, TieJun Zhang**

Department of Mechanical and Materials Engineering, Masdar Institute, Khalifa University of Science and Technology, P.O. Box 54224, Abu Dhabi, UAE

*Email: tjzhang@masdar.ac.ae